Metallography, Microstructure, and Analysis (2022) 11:761–773
https://doi.org/10.1007/s13632-022-00888-1

PEER-REVIEWED PAPER

Microstructure and Mechanical Properties of Ti Particles Reinforced AZ31-Mg Alloy Matrix Composites Through ARB and Subsequent Annealing

Baleegh Alobaid[1]

Received: 25 March 2022 / Revised: 1 September 2022 / Accepted: 6 September 2022 / Published online: 23 September 2022

Abstract
This work aims to study the effects of dispersed pure titanium particles (150 mesh) with 0, 2.3, 3.5, 4.9, and 8.6 wt.% on the microstructure and mechanical properties of AZ31-Mg alloy matrix. Mg–Ti composites were processed through a three accumulative roll bonding (ARB) process using thickness reductions of 50% each pass followed by heat treatment at 400 °C for 12 h in an argon atmosphere. Mechanical properties of Mg–0 and Mg–2.3 Ti composite were enhanced by ~ 8 and 13% in YS and ~ 30 and 32% in UTS, respectively. Meanwhile, the elongation of the composite was decreased by 63 and 70%. After heat treatment, the results showed a decrease in yield strength and increased in the elongation to fracture. The mechanical properties of the Mg–0 and Mg–2.3 Ti composite were enhanced; ultimate tensile strength by 9 and 7%, and elongation by 40 and 67%, while the yield strength was decreased by 28 and 36% compared with the initial AZ31. Enhancement of strength and ductility was developed based on the operation of two mechanisms: developing a random matrix texture by ARB, and dispersion of ductile titanium particles. ARB is an efficient process to fabricate an Mg–Ti composite material.

Keywords AZ31 matrix · Ti particles · Accumulative roll bonding (ARB) · Mechanical behavior · Heat treatment

Introduction

Magnesium is lighter than aluminum and steel by 35 and 78%, respectively. Magnesium-based composite materials have become more attractive in the transportation industry and aerospace applications due to their combined desirable properties such as lightweight, high strength, and high recyclability. Magnesium alloy AZ31 (Mg–3%Al–1%Zn) has been used in industrial applications because of its good mechanical properties, damping characteristics, machinability, and low casting costs [1–3]. However, it is difficult to form Mg alloys at an ambient temperature because Mg alloys have a hexagonal close-packed (HCP) structure [4], and the axial ratio(c/a) is 1.624 smaller than the ideal value[5]. Only the basal slip system is active at room temperature, while the other slip systems (prismatic and pyramidal) are inactive. Therefore, insufficient plastic deformation occurs at room temperature [6–9]. During severe plastic deformation processing high temperature (i.e., hot rolling and extrusion), other non-basal slip systems or twinning systems are activated. In general, HCP materials have slip systems: basal $\{0001\}<11\bar{2}0>$, prismatic $\{10\bar{1}0\}<11\bar{2}0>$ and pyramidal $\{10\bar{1}1\}<11\bar{2}0>$ [10, 11]. Therefore, the texture control is an effective way to enhance the ductility of Mg and its alloys at room temperature [12]. Severe plastic deformation (SPD) is a process in which a large strain is applied at a temperature below recrystallization temperature without thermal treatment to produce ultrafine-grained (UFG) structures. There are several processes which have been developed to produce high strain in metals accompanied with changes in sample dimensions such as equal-channel angular pressing (ECAP), high-pressure torsion (HPT), multi-axial forging (MAF), and accumulative roll bonding (ARB) [7, 13–16].

Composite materials are alternating which have significant advantages due to the combination of their desirable properties, such as strength and ductility. Ceramic and intermetallic compounds were employed as reinforcements to Mg- alloys such as SiC, TiC and TiB_2, Al_20_3, and graphene nano-platelets [17–21]. However, all of these hard and brittle reinforcements lead to a decrease in the ductility of the

✉ Baleegh Alobaid
Baleegh.saud@mu.edu.iq

[1] College of Engineering, Al-Muthanna University, Samawah, Muthanna 66001, Iraq

composites[22]. Alam et al. [23] claimed that there is an improvement in the microstructure and mechanical properties of AZ41 and AZ50 Mg alloys by adding nano-sized Al_2O_3 particles and Ca. Mg-based composites can improve formability and toughness by the dispersion of ductile particles, which are deformed plastically with stress lower than the maximum strength of the Mg matrix. The dispersion particles prevent stress concentration and cracking at Mg grain boundaries. Ti has been reported as a suitable dispersoid because it has a very low solid solubility, and there is no affinity and no intermediate reaction layer in the Mg–Ti binary phase diagram [5, 22, 24–26]. Kitazono et al. [2] synthesized Mg/Ti composites by accumulative diffusion-bonding (ADB). The mechanical properties of the AZ91Mg alloy were improved by the dispersion of Ti particles in the AZ91matrix. They suggested that the development of a random texture improved ductility due to severe plastic deformation and stress relaxation in Ti particles. Esen et al. [27] prepared Ti–Mg composite rods by hot rotary swaging from elemental powders of titanium and magnesium. The composite was in vivo tested in Ringer's solution which can be used in the human body. In this study, Ti particles (0, 2.3, 3.5, 4.9, and 8.6 wt.%) were used to improve AZ31 ductility. We proposed the accumulative roll bonding (ARB) process which is known as a useful severe plastic deformation technique to fabricate metal–metal composites material. The materials synthesized were studied for microstructural and mechanical properties. The reinforced composites with Ti particles were compared to that of unreinforced samples.

Materials and Experimental Procedures

AZ31 magnesium alloy (Mg–3wt.% Al–1 wt.% Zn, provided by Magnesium Elektron) was used as a matrix, and high purity (99.9%) titanium particles (spherical − 150 mesh, provided by Alfa Aesar) were added as ductile reinforcements. Mechanical properties of the AZ31 matrix are 224–227 MPa yield strength, 290–291 Mpa ultimate tensile strength, and 17% elongation. The AZ31 sheet was 0.80 ± 0.1 mm in thickness. The samples were 25 mm in width 50 mm in length, and 0.80 ± 0.1 mm in thickness (5ply plates) of the AZ31 with five weight percentage of Ti 0, 2.3, 3.5, 4.9, and 8.6 as starting materials. The samples were named as (Mg–0 Ti, …, Mg–8.6 Ti) in correspondence to the Ti weight percentage in the composite. Before stacking the AZ31 layers, the Ti particles were distributed on the bonding interface. First, the samples were assembled by the uniaxial hot press with a load of 5 tons at 300 °C for 20 min to bond the AZ31 layers and avoid Ti particles oxidation [2]. Opposite corners of the assembled samples were fastened tightly by steel wires to prevent sliding of the AZ31 layers during ARB. Second, the assembly samples were heated in an argon atmosphere furnace at 450 °C for 15 min, and then, three ARB cycles were done using thickness reductions of 50% each pass [13]. The detailed schematic diagram of the ARB process is illustrated in Fig. 1.

The ARB process was carried out without lubricant using rolling mills with 101.15 mm diameter. After each ARB cycle, the sample was cut into two halves using a shear cutting machine, surface treatment, assembly, and rolled [28, 29]. To achieve good bonding between layers, the AZ31 plates were decreased by an ultrasound bath using acetone for 15 min and roughened using a rotating "stainless steel" wire brush [30–32]. Surface treatment was done for the assembly samples and between the ARB cycles. Heat treatment was carried out at 400 °C for 12 h in an argon atmosphere. Optical microscopy (OM), X-ray diffraction (XRD), scanning electron microscopy (SEM), energy dispersive spectroscopy (EDS), electron backscatter diffraction (EBSD), nanoindentation, and tensile tests were used to characterize the samples before and after heat treatment. The samples were mounted using a non-conductive epoxy. The surface was prepared using silicon carbide abrasive papers for grinding and MasterPolish (0.05 µm) polishing liquid with a ChemoMet cloth for mechanical polishing. Electrochemical polisher was used to polish AZ31 matrix; an electrolyte (methanol: ethanol: nitric acid = 10:10:3) at room temperature and voltage of 27–30 V to obtain high-quality EBSD patterns [33, 34]. EBSD was performed on the as-rolled and annealed samples Mg–0 Ti and Mg–4.9 Ti using FEI (Helios NanoLab 660) equipped with an electron backscatter diffraction (EBSD) system. The EBSD data were analyzed using HKL channel 5 software. Hardness was evaluated by nanoindentation (Agilent G200). The tensile tests conducted at room temperature with a strain rate of 0.5 mm/min. Tensile specimens with 10 mm gauge length were machined by an electric discharge machine (EDM) in rolling direction (RD) [35].

Archimedes' principle was used to measure the density of the Mg–Ti composites. Table 1 lists the density of the prepared Mg–Ti composites, which increases with the increase of the weight fraction of Ti particles, as expected. The volume percentage of Ti was calculated using below formula:

$$\frac{\frac{\text{wt.\% of Ti}}{\text{density of Ti}}}{\frac{\text{wt.\% of Ti}}{\text{density of Ti}} + \frac{\text{wt.\% of AZ31 matrix}}{\text{density of AZ31 matrix}}}$$

Results and Discussion

Optical micrographs of the ARBed Mg–4.9 composites materials are shown in Fig. 2. It can be seen the bonding line and agglomeration of the Ti particles in the first ARB

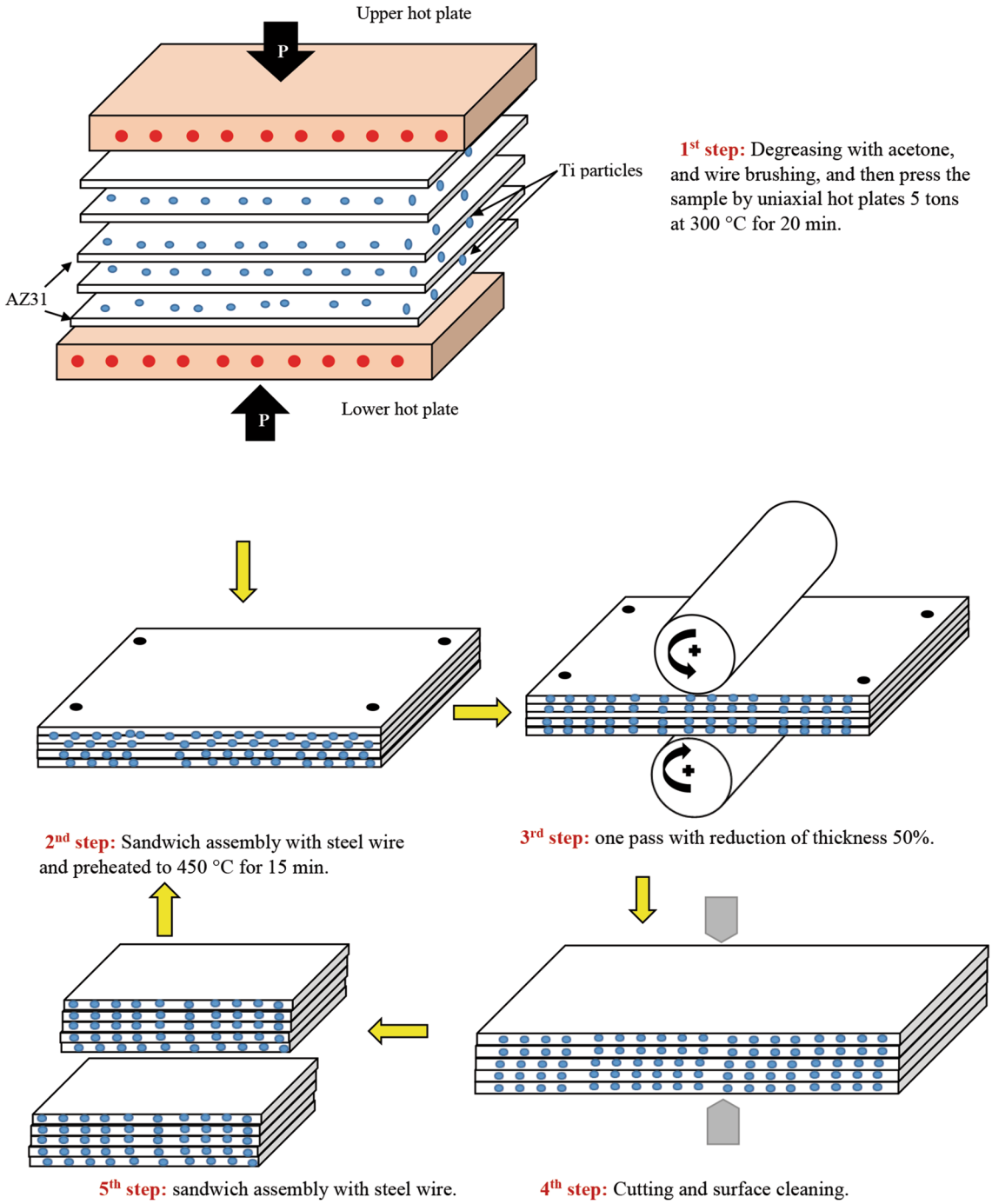

Fig. 1 Schematic diagram of the ARB process

cycle (Fig. 2a). The Ti particle distribution in the AZ31 matrix became more uniform after the second and third ARB cycles, as shown in Fig. 2b–d. The bonding lines disappeared after the three ARB cycles which indicate that ARB is an effective process to fabricate Mg–Ti composite material [9, 15, 36, 37]. In this study, several weights percentages of Ti particles (0, 2.3, 3.5, 4.9, and 8.6) were added to the AZ31 matrix. The microstructures of the AZ31-Ti composite with four different weight contents of Ti after three ARB cycles are shown in Fig. 3. The composite material showed no visual defects such as interface debonding, cracks, or pores after three ARB cycles for both AZ31/AZ31 and Ti/AZ31 interfaces.

The Ti particles were quite uniformly distributed without agglomeration in the matrix; neither clusters of Ti particles nor new phases were created during the ARB process [22,

26]. Figure 4 shows X-ray diffraction patterns of AZ31, Ti-particles, Mg–4.9 Ti, and Mg–4.9 Ti in annealed condition after three ARB cycles.

Furthermore, no changes of the Ti particle shape or particle size were detected during ARB cycles. This is related to the high strength of Ti, and the flow deformation of the matrix is not enough to deform the Ti particles. It has been reported that the particles shape and size may affect the mechanical properties of the composite materials [2, 26]. In this work, the Ti reinforcement particles found with round edges, and therefore, no stress concentration would occur due to sharp edges[38, 39]. The total reduction and equivalent plastic strain can be calculated from Eqs. 1 and 2 [40, 41].

Table 1 The density of the prepared Mg–Ti composites

Material	Ti particles		Density (g/cm^3)
	wt.%	vol.%	
Mg-0 Ti	0	0	1.7700 ± 0.0006
Mg-2.3 Ti	2.3	0.9	1.7952 ± 0.0019
Mg-3.5 Ti	3.5	1.4	1.8089 ± 0.0055
Mg-4.9 Ti	4.9	2	1.8240 ± 0.0030
Mg-8.6 Ti	8.6	3.6	1.8685 ± 0.0043

$$\text{Total reduction } (\%) = \left(1 - \frac{1}{2^n}\right) \times 100 \quad (1)$$

$$\text{Equivalent plastic strain } \varepsilon = n\left(\frac{2}{\sqrt{3}}\right) \ln\left(\frac{1}{2}\right) = 0.8n \quad (2)$$

where n is the number of ARB cycles.

To study the effect of Ti addition on the AZ31 matrix texture, EBSD was conducted for the as-ARBed and annealed condition for the Mg–0 Ti and Mg–4.9 Ti samples after three ARB cycles. The results of texture analysis based on the EDSD scan were performed on the TD plane. SEM images and pole figures corresponding to the AZ31 matrix of a composite structure Mg–0 Ti and Mg–4.9 Ti are shown in Fig. 4. Dynamic recrystallization (DRX) has taken place in the AZ31 matrix where recrystallized grains grew by the migration of grain boundaries during the ARB process. As shown in Fig. 5a, the microstructure of Mg–0 Ti was populated by recrystallized grains. In addition, heating between ARB passes may cause partial recrystallization

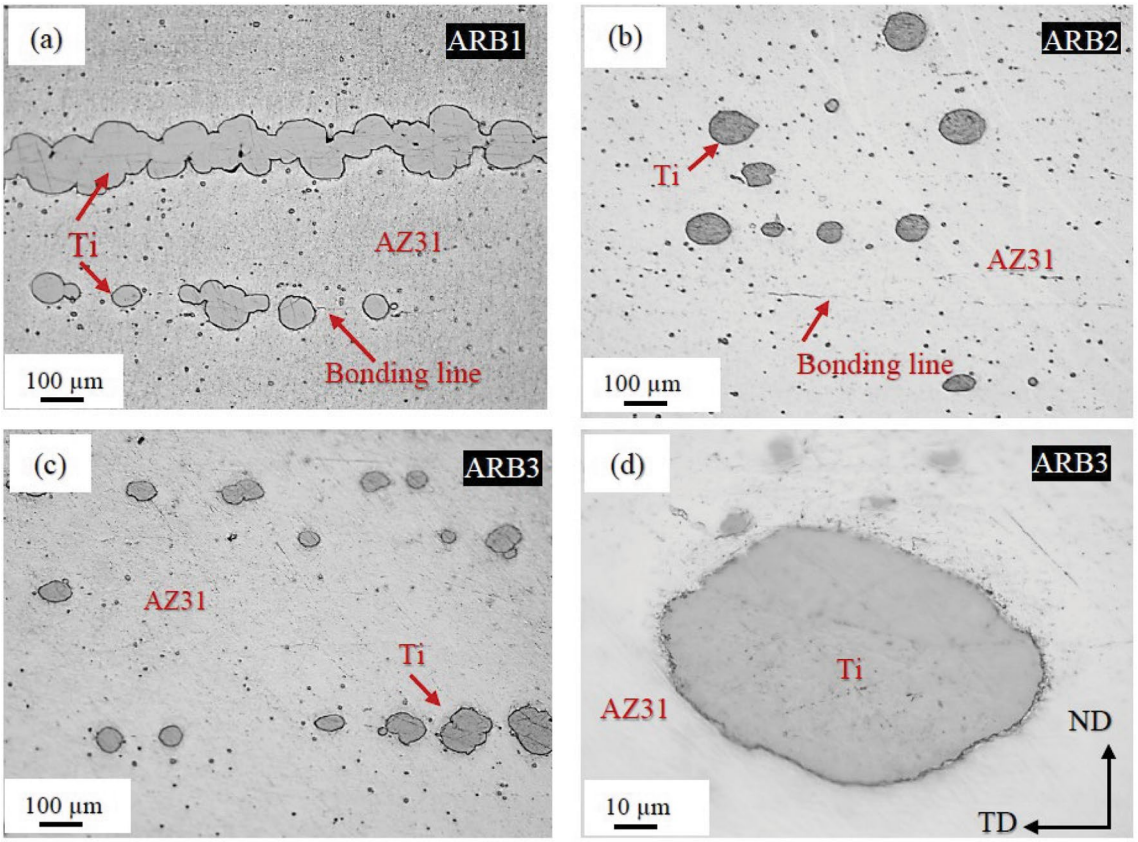

Fig. 2 Microstructure of the Mg–4.9Ti composite processed by accumulative roll bonding. (**a**) ARB1, (**b**) ARB2, (**c**) ARB3, (**d**) high magnification of (**c**)

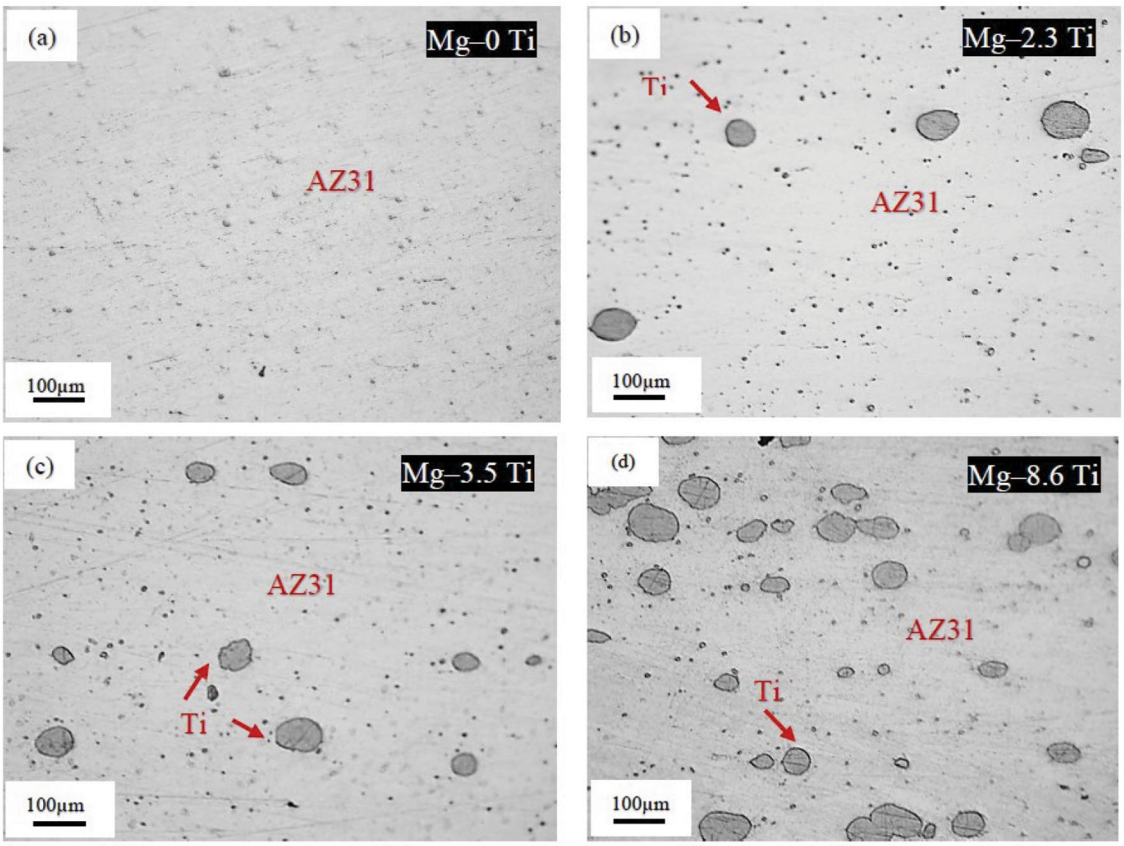

Fig. 3 The microstructure of the composite processed by three ARB passes. (**a**) Mg–0 Ti, (**b**) Mg–2.3 Ti, (**c**) Mg–3.5 Ti, and (**d**) Mg–8.6 Ti

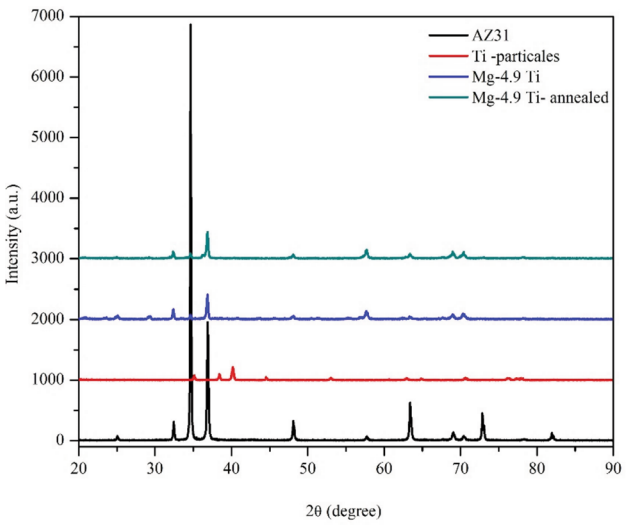

Fig. 4 Shows X-ray diffraction patterns of AZ31, Ti- particles, Mg–4.9 Ti, and Mg–4.9 Ti annealed

and remove the accumulated strain [9, 15]. The (0001) PF showed strong basal texture with maximum pole intensity of 16.04, which tilted at 15° away from normal direction ND toward TD, as shown in Fig. 5a-1. Zhan et al. [9, 15] have reported improved mechanical properties of the AZ31 after three ARB cycles at 300 and 400 °C with 50% reduction. According to them, the basal texture was weakened as a result of repeating the ARB process and the DRX, which agrees with my research results.

To further understand the effect of Ti particles (Mg–4.9 Ti) on the AZ31 matrix texture, the EBSD scan was conducted at two sites. Site1 was in areas without Ti particles and site2 around Ti particles, as shown in Fig. 4b and c, respectively. Recrystallized grains were found in the site1 which is similar to Mg–0 Ti matrix, as shown in Fig. 5b. Also, the (0001) PF showed a strong basal texture with maximum pole intensity of 12.63 and tilted at 15° away from ND toward TD, as shown in Fig. 5b-1. Pérez et al. [25] have studied Mg–Ti composites (5 to 15 vol.% of Ti) processed by powder metallurgy followed by hot extrusion at 400 °C. According to them, the basal texture intensity decreased with increasing Ti volume fraction. Elongated matrix grains formed in the vicinity of the Ti particles in site2 (Fig. 5c), which means a strong interaction between AZ31 and Ti particles during the ARB process. The Ti particles resist the AZ31 deformation flow that leads to forming the AZ31 fiber texture around Ti particles [22, 26]. The site2 showed a strong basal texture with maximum pole intensity of 15.12

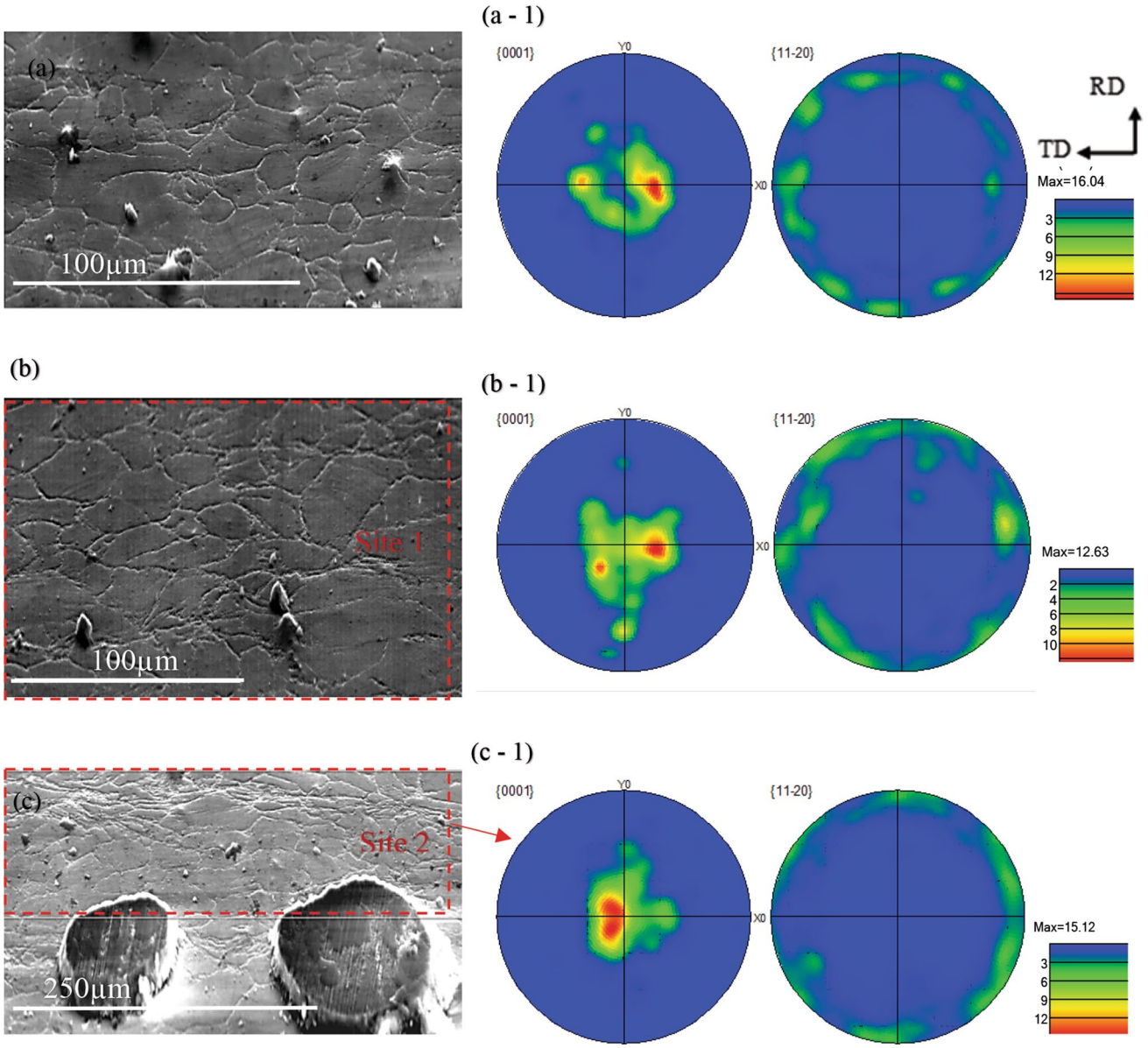

Fig. 5 SEM and pole figures corresponding to AZ31 matrix after three ARBed cycles: (**a**) Mg–0 Ti, (**b**) Mg–4.9 Ti site 1, (**c**) Mg–4.9 Ti site 2

and − 5° away from normal direction ND toward TD, as shown in Fig. 5c-1. The Ti particle zones were disturbed by the texture to re-arrange. In addition, Ti particles are located between the stacking AZ31 sheets during the ARB process, so that the texture changes from rolling texture to the large shear texture (site2) between bonded surfaces [42]. Thus, the AZ31 texture intensity is high in the vicinity of the Ti particles.

Heat treatment was carried out at 400 ℃ for 12h to relive the internal stress in the matrix during the ARB process. EBSD was used to analysis the texture changes after post-heat treatment. Figure 6 shows SEM images and the pole figures of the Mg–Ti composites with Mg–0Ti and Mg–4.9 Ti after three ARB passes. Static recrystallization (SRX) and grain growth occurred upon heat treatment. As shown in Fig. 6a–c, the grains become larger and more equiaxed, and the matrix fiber texture around the Ti particles disappeared. Furthermore, the basal texture intensity was weakened due to static recrystallization during heat treatment. The comparison of the pole figures of the ARBed and annealed samples reveals that the heat treatment has significantly influenced the texture intensity. The basal texture intensity of the Mg–0Ti sample was reduced from 16.04 to 7.16. The (0001) PF shows multi-basal poles along the TD, as shown in Fig. 6a-1. Also, the EBSD was conducted in two sites for the sample with Mg–4.9 Ti. Site1 shows lower

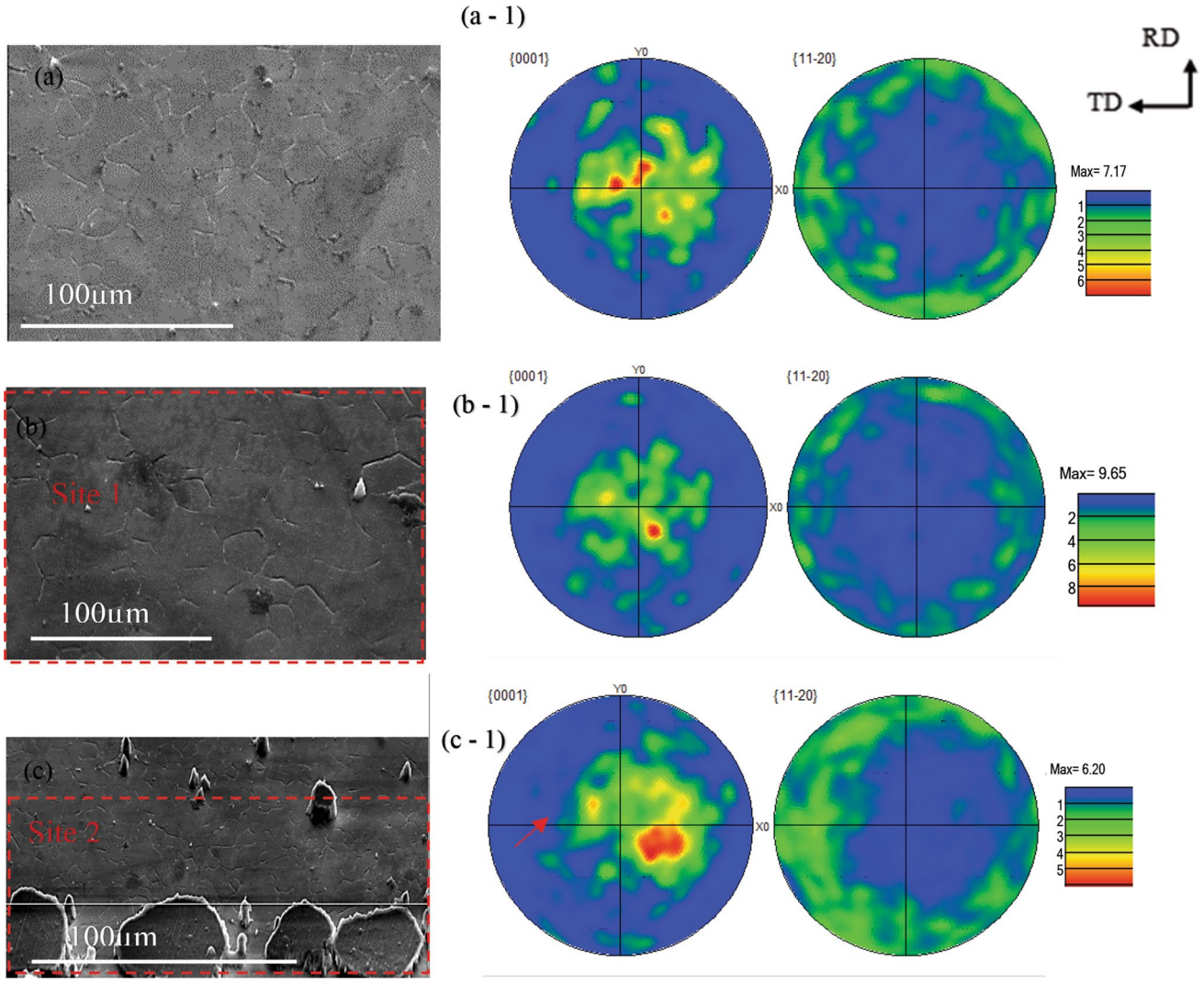

Fig. 6 SEM and pole figures corresponding to AZ31 matrix after three ARBed cycles and annealing heat treatment: (**a**) Mg–0 Ti, (**b**) Mg–4.9 Ti site 1, (**c**) Mg–4.9 Ti site 2

basal texture intensity than the as-rolled condition where the (0001) PF reduced from 12.63 to 9.65 (Fig. 6b-1), while the site2 (0001) PF was reduced from 15.12 to 6.20, as shown in Fig. 5c-1.

Figure 7 depicts the EDX line scan profile of the annealed Mg–4.9 Ti composite, which reveals a diffusive zone around the Ti particle. The spatial distribution of the concentrations of Ti and Mg can be seen clearly, suggesting the presence of inter-diffusion across the Mg/Ti interfaces and the diffusion-assisted interface bonding [3].

Nanoindentation measurements were conducted on polished samples before and after heat treatment. Berkovich indenter was used with a test load of 30 gf and a dwell time of 15 s. The hardness tests were conducted randomly on the Mg–Ti composite material, and the averages of the values were reported. Figure 8 shows the room temperature results of the nanoindentation measurements of as-received AZ31 and Mg–Ti composite materials reinforced with different Ti contents. The result reveals that the hardness values were significantly increased after three ARB cycles compared to initial hardness of the AZ31. In addition, the hardness values increased with an increase in the weight percentage of Ti content in the matrix. The hardness value was 0.85, 0.95, and 1.025 GPa for the as-ARBed condition of the Mg–0 Ti, Mg–4.9 Ti, and Mg–8.6 Ti, respectively. The hardness of the unreinforced Mg–0 Ti and Mg–4.9 Ti has increased by about 43% and 60%, respectively, compared to the AZ31. This is attributed to: (a) grain refining during ARB, (b) the formation of localized plastic deformation (fiber texture) around the Ti particles, which was caused by plastic deformation incompatibility between the reinforcement and matrix, and (c) the presence of relatively harder phase Ti particles in the

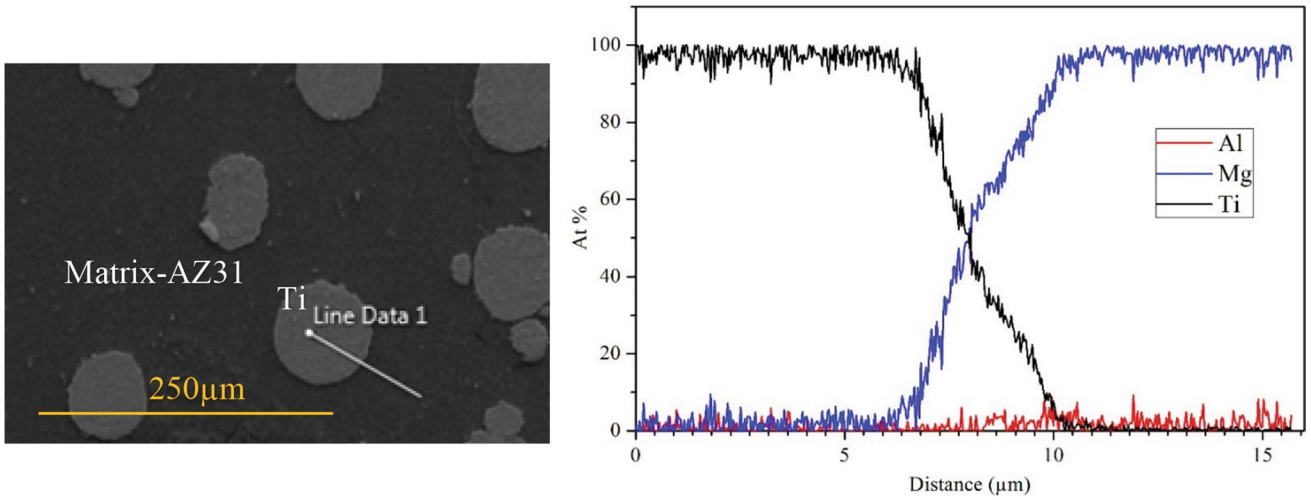

Fig. 7 EDX line-scan profiles off annealed Mg–4.9 Ti

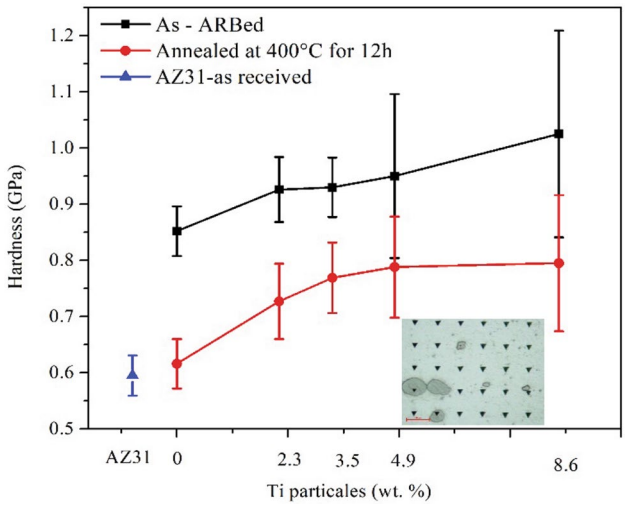

Fig. 8 Nanoindentation measurements of as-received AZ31 and Mg–Ti composite material reinforced with different Ti contents

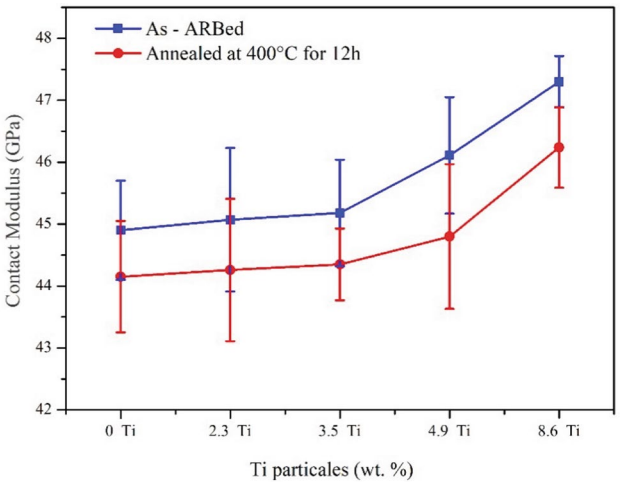

Fig. 9 Contact modulus of Mg–Ti composites

matrix [22, 26, 38, 43]. Furthermore, the internal stresses developed in the metal matrix composite materials, which caused by various factors. It has been reported that the increase of the Ti particle fraction leads to increase in internal stress between Ti reinforcement and matrix due to the differences in their thermal expansion coefficients and the modulus of elasticity [44, 45].

Softening behavior and stress relieve upon heat treatment of the metal matrix composite materials were investigated [46, 47]. Figure 8 shows the hardness as a function of Ti content in the matrix. The hardness decreased after heat treatment at 400 °C for 12 h. This may be attributed to the relaxation of the internal stress and grain coarsening during heat treatment. It can be seen that the recrystallization has changed the texture of the ARBed materials completely (Figures 5, 6). The hardness values were 0.61, 0.78, and 0.79 GPa for the Mg-0, Mg-4.9, and Mg-8.6 wt.% Ti, respectively. The hardness of the as-received AZ31 increased by ~ 3.5% and 32.5% compared to Mg-0 Ti and Mg–4.9 Ti, respectively.

Figure 9 shows the variation of the contact modulus, as calculated from the unloading curves of the nanoindentation tests, with the weight fraction of Ti particles. The contact modulus increases with the increase of the weight fraction of Ti particles, as expected, due to the large modulus of Ti. The annealing of the as-ARBed Mg–Ti composites led to a slight decrease in the contact modulus of the corresponding composites. Such a difference is statistically insignificant.

Figure 10 presents the tensile behavior of the Mg–Ti composites after three ARB passes with and without annealing.

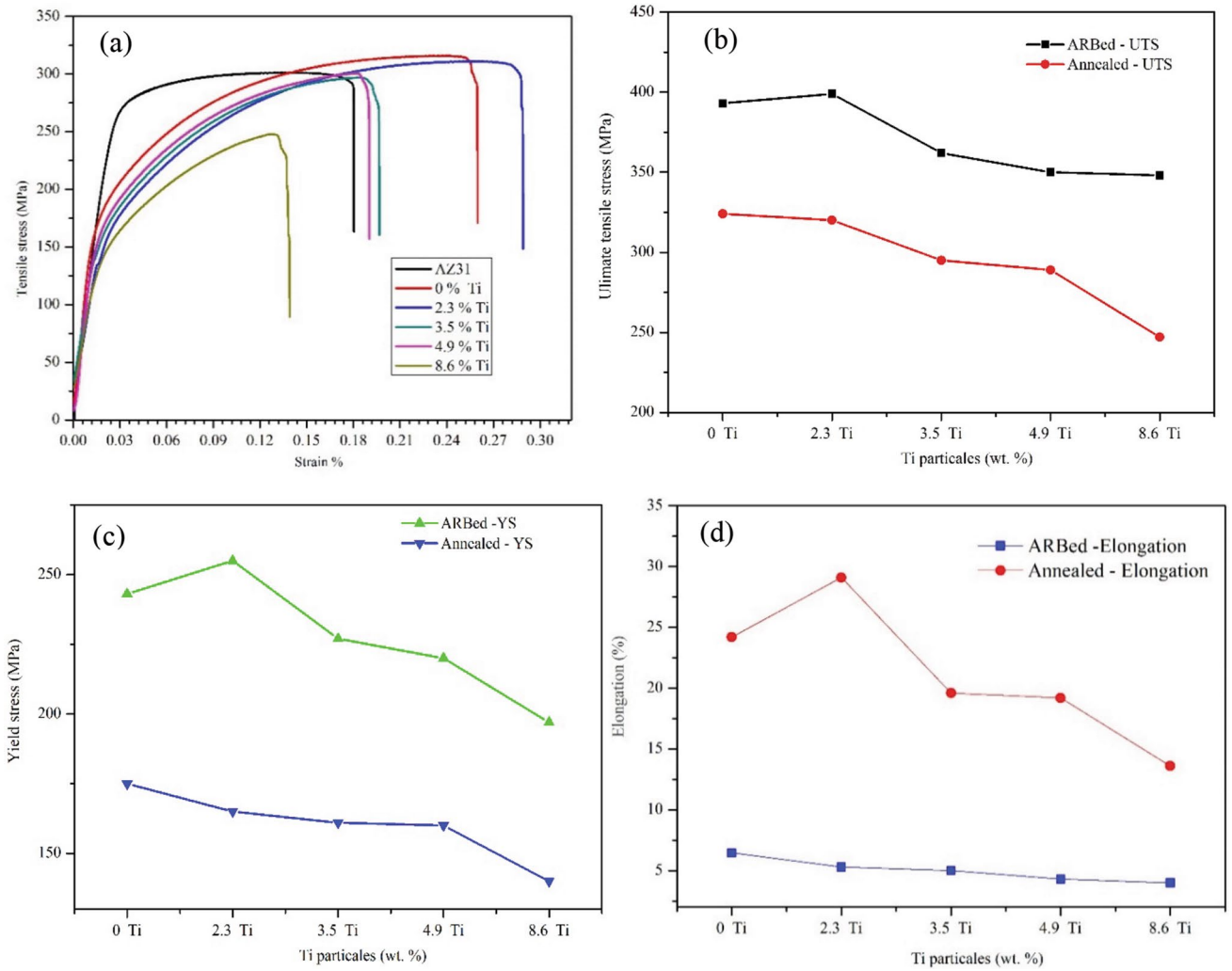

Fig. 10 Tensile behavior of Mg–Ti composite materials: (**a**) stress–strain curves, (**b**) ultimate tensile strength, (**d**) yield stress, and (**d**) elongation

The ARB processing caused the increase of the ultimate tensile strength (UTS) and 0.2% yield strength (YS) of the Mg–Ti composites. However, both the ultimate tensile strength (UTS) and 0.2% yield strength (YS) as well as the elongation generally decrease with the increase of the weight fraction of Ti particles, except Mg–2.3 Ti. Such behavior might be associated with the bonding strength between Ti particles and the AZ31 matrix. Also, stress concentration around Ti particles under tension might cause local damage when local stress is higher than the bonding strength. The combinational effect of the bonding strength and the local damage likely contributes to the decrease of the mechanical strength of the Mg–Ti composites for the weight fraction of Ti particles larger than 2.3 wt.% [24].

The annealing-induced decrease of the mechanical strength and the increase in elongation are consistent with the annealing-induced decrease of the indentation hardness. This change can be attributed to (a) the relief of residual stresses in the matrix around Ti particles, (b) an increase in average grain size, and (c) a reduction of the basal texture intensity due to SRX.

Table 2 summarizes the comparison of the tensile properties of AZ31 and Mg-based composites reinforced with hard and ductile particles, such as SiC, Al_2O_3, and Ti, available in the literature. It is evident that ARB is a relatively better process for making Mg–Ti composites than the other processes available in the literature.

Figure 11 shows the fractured surface of the annealed Mg–0 Ti, Mg–2.3 Ti, and Mg–8.6 Ti tensile samples. There are dimples presented on the fracture surfaces, suggesting ductile fracture. Ti particles in Mg–2.3 Ti and Mg–8.6 Ti samples are observed on the fractured surfaces, suggesting poor bonding between Ti particles and the AZ31 matrix. This result confirms decreasing in the mechanical strength of Mg–Ti composites due to limited load transfer between the Mg matrix and Ti particles. However, the SEM image for the

Table 2 Comparison between this study and the literature of Mg–Ti composite materials

Material	Method of Preparation	0.2% YS (MPa)	UTS (MPa)	Elongation (%)
AZ31B		225	302	17.4
Mg–0 Ti [Present study]	ARB	243	393	6.47
	ARB and annealed	175	324	24.2
[Present study]Mg -2.3 Ti	ARB	255	399	5.3
	ARB and annealed	165	320	29.1
Mg[Present study]-3.5 Ti	ARB	227	362	5
	ARB and annealed	161	295	19.6
Mg–4.9 Ti [Present study]	ARB	220	350	4.3
	ARB and annealed	160	289	19.2
Mg–8.6 Ti [Present study]	ARB	197	348	4
	ARB and annealed	140	247	13.6
ZK51 [48]	Hot extrusion	229	315	8.5
ZK51-SiC		302	355	3.2
ZK51-Ti		295	386	16.9
Mg [25]	Hot extrusion	233 ± 3	256 ± 3	4 ± 0.5
Mg–5 Ti		201 ± 5	223 ± 10	5.5 ± 1
Mg–10 Ti		200 ± 4	225	6 ± 1
Mg–15 Ti		196 ± 5	215 ± 8	5 ± 1
Mg–0 Ti[22]	Spark plasma sintering and hot extrusion	182	223	14.3
Mg–1 Ti		180	221	16.1
Mg–3 Ti		184	224	14.9
Mg–5 Ti		179	218	15.5
AZ31B/ Al_2O_3[49]	Hot extrusion	204 ± 8	317 ± 5	22 ± 2.4
AZ31 matrix [18]	Hot rolling	208	269	16.9
AZ31-SiC		258	308	5.4

Mg–2.3 Ti sample (Fig. 11d) reveals the extension of cracks from the Mg matrix to a Ti particle, indicating load transfer from the AZ31 matrix to the Ti particle. This can increase the strength of the composite due to the increase in the loading capacity by the Ti particles, suggesting the benefit of ductile reinforcements to the AZ31 matrix in comparison to hard-particle reinforcements [50, 51].

Conclusions

The Ti particle dispersion AZ31 was successfully processed through ARB process. The microstructure and mechanical properties were evaluated. The results can be summarized as follows:

1. Mg–Ti composite materials with different Ti content (Mg–0 to Mg–8.6 Ti) can successfully be made by ARB. Addition of Ti particles improves the UTS, 0.2%YS, and degrades the ductility of the composite for as-ARBed condition, whereas post-heat treatment leads to significant decrees of the UTS, 0.2% YS and a significant increase of the ductility to fracture.
2. Detailed texture studies using EBSD analysis revealed recrystallization and residual stress relieve due to heat treatment when compared to the as-ARBed (non-heat treated composites).
3. Mechanical properties of the heat-treated composites showed a significant increase in ductility with a reduction in yield strength which is caused by texture weakening due to matrix recrystallization.
4. Ti particle-reinforced magnesium and its alloys can be superior to that of using hard reinforcing particles such as SiC and Al_2O_3.
5. The fracture of Ti particles was the main failure mechanism in the Mg/Ti composites.
6. Ti particles could be used as ductile reinforcement for the ductility of magnesium matrix composite materials.

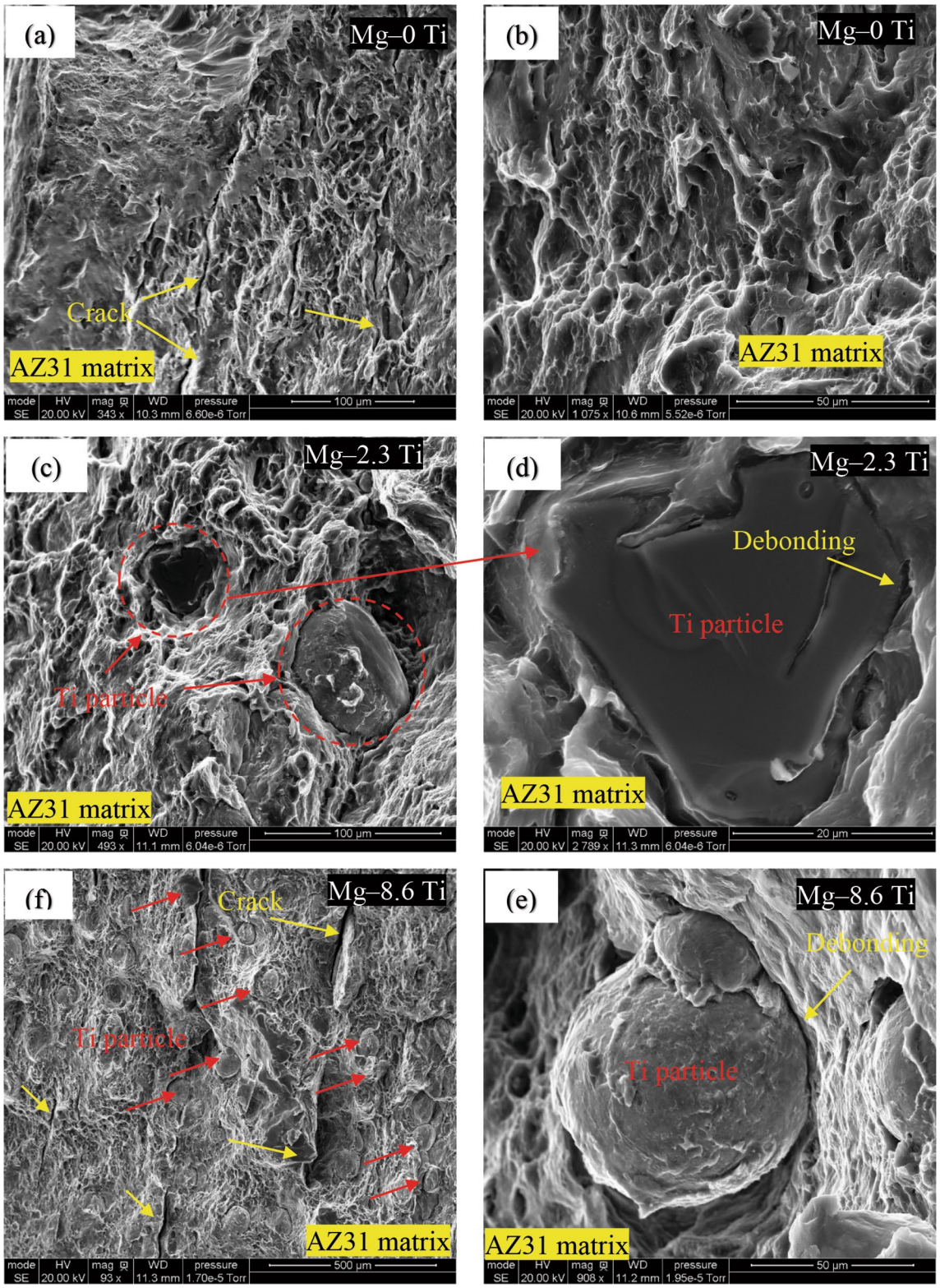

Fig. 11 SEM of fractured surface of tensile test samples for heat treated sample: (**a**, **b**) Mg–0 Ti, (**c**, **d**) Mg–2.3 Ti, and (**e**, **f**) Mg–8.6 Ti

Acknowledgments This study was partially supported by the Higher Committee for Education Development (HCED) in Iraq and the University of Kentucky. The author is grateful to acknowledge the helpful discussions with Prof. Yang-Tse Cheng and Fuqian Yang with thanks.

References

1. H. Somekawa, H. Hosokawa, H. Watanabe, K. Higashi, Diffusion bonding in superplastic magnesium alloys. Mater. Sci. Eng. **A339**, 328–333 (2003)
2. K. Kitazono, S. Komatsu, Y. Kataoka, Mechanical properties of titanium particles dispersed magnesium matrix composite produced through accumulative diffusion bonding process. Mater. Trans. **52**(2), 155–158 (2011)
3. B. Alobaid, F. Yang, Y.-T. Cheng, Microstructure and deformation behavior of hot-rolled AZ31/Ti multilayers. Mater. Res. Express. **6**(8), 08652 (2019)
4. T.B. Britton, F.P.E. Dunne, A.J. Wilkinson, On the mechanistic basis of deformation at the microscale in hexagonal close-packed metals. Proc. R. Soc. A. Math. Phys. Eng. Sci. **471**(2178), 20140881 (2015)
5. H. Kawamoto et al., Analysis of strain transfer through the Mg/Ti interface using crystallographic orientation analysis based on electron back-scattered diffraction patterns. Mater. Trans. **49**(5), 1107–1111 (2008)
6. H.K. Kim, W.J. Kim, Microstructural instability and strength of an AZ31 Mg alloy after severe plastic deformation. Mater. Sci. Eng. A. **385**(1–2), 300–308 (2004)
7. Y. Miyahara, Z. Horita, T.G. Langdon, Exceptional superplasticity in an AZ61 magnesium alloy processed by extrusion and ECAP. Mater. Sci. Eng. A. **420**(1–2), 240–244 (2006)
8. J.A. Del Valle, F. Carreño, O.A. Ruano, Influence of texture and grain size on work hardening and ductility in magnesium-based alloys processed by ECAP and rolling. Acta Mater. **54**(16), 4247–4259 (2006)
9. M.Y. Zhan et al., Microstructure and mechanical properties of Mg–Al–Zn alloy sheets severely deformed by accumulative roll-bonding. J. Mater. Sci. **42**(22), 9256–9261 (2007)
10. F.D. Dumitru, G. Deák, O.F. Higuera-Cobos, J.M. Cabrera-Marrero, Effect of severe plastic deformation on an extruded ZK60 magnesium alloy. MRS Online Proceedings Library Archive . **1818,** Imrc2015s4g-p004 (2016)
11. K. Asano, H. Enoki, E. Akiba, Synthesis process of Mg–Ti BCC alloys by means of ball milling. J. Alloys Compd. **486**(1–2), 115–123 (2009)
12. Q. Yang et al., Effect of multi-pass bending deformation on microstructure evolution and mechanical properties of AZ31 alloy sheet. Mater. Res. **19**(2), 322–327 (2016)
13. M. Zhan, C. Li, D. Zhang, W. Zhang, Processing of AZ31 magnesium alloy by accumulative roll-bonding at gradient temperature. Acta Metall. Sin. (English letters). **25**(1), 65–75 (2012)
14. Q.D. Wang, Y.J. Chen, J.B. Lin, L.J. Zhang, C.Q. Zhai, Microstructure and properties of magnesium alloy processed by a new severe plastic deformation method. Mater. Lett. **61**(23), 4599–4602 (2007)
15. M.-Y. Zhan, Y.-y Li, W.-p Chen, Improving mechanical properties of Mg–Al–Zn alloy sheets through accumulative roll-bonding. Trans. Nonferrous Metals Soc China. **18**(2), 309–314 (2008)
16. M.T. Pérez-Prado, J.A. del Valle, O.A. Ruano, Effect of sheet thickness on the microstructural evolution of an Mg AZ61 alloy during large strain hot rolling. Scripta Mater. **50**(5), 667–671 (2004)
17. M.P. Reddy et al., Enhanced performance of nano-sized SiC reinforced Al metal matrix nanocomposites synthesized through microwave sintering and hot extrusion techniques. Prog. Nat Sci. Mater. Int. **27**, 606–614 (2017)
18. X. Wang et al., Microstructural modification and strength enhancement by SiC nanoparticles in AZ31 magnesium alloy during hot rolling. Mater. Sci. Eng. A. **715**, 49–61 (2018)
19. P. Kumar, et al., Strength of Mg–3%Al alloy in presence of graphene nano-platelets as reinforcement. Mater. Sci. Technol. 1086–1095 (2018)
20. Z. Xiuqing et al., The mechanical properties of magnesium matrix composites reinforced with (TiB2+TiC) ceramic particulates. Mater. Lett. **59**(17), 2105–2109 (2005)
21. M. Paramsothy et al., Enhancing tensile/compressive response of magnesium alloy AZ31 by integrating with Al2O3 nanoparticles. Mater. Sci. Eng. A. **527**(1–2), 162–168 (2009)
22. J. Umeda, M. Kawakami, K. Kondoh, E.L.-S. Ayman, H. Imai, Microstructural and mechanical properties of titanium particulate reinforced magnesium composite materials. Mater. Chem. Phys. **123**, 649–657 (2010)
23. M.E. Alam et al., Improving microstructural and mechanical response of new AZ41 and AZ51 magnesium alloys through simultaneous addition of nano-sized Al_2O_3 particulates and Ca. J. Alloys Compd. **574**, 565–572 (2013)
24. S.F. Hassan, M. Gupta, D evelopment of ductile magnesium composite materials using titanium as reinforcement. J. Alloys Compd. **345**, 246–251 (2002)
25. P. Pérez, Influence of titanium volume fraction on the mechanical properties of Mg–Ti composites. Int. J. Mater. Res. **100**(3), 366–369 (2009)
26. P. Pérez, G. Garcés, P. Adeva, Mechanical properties of a Mg–10 (vol.%)Ti composite. Compos. Sci. Technol. **64**(1), 145–151 (2004)
27. Z. Esen et al., Titanium–magnesium based composites: mechanical properties and in-vitro corrosion response in Ringer's solution. Mater. Sci. Eng. A. **573**, 119–126 (2013)
28. Y. Saito, H. Utsunomiya, N. Tsuji, T. Sakai, Novel ultra-high straining process for bulk materials—development of the accumulative roll-bonding (ARB) process. Acta Mater. **47**(2), 579–583 (1999)
29. H.S. Liu, B. Zhang, G.P. Zhang, Microstructures and mechanical properties of Al/Mg Alloy multilayered composites produced by accumulative roll bonding. J. Mater. Sci. Technol. **27**(1), 15–21 (2011)
30. L. Li, K. Nagai, F. Yin, Progress in cold roll bonding of metals. Sci. Technol. Adv. Mater. **9**(2), 023001 (2008)
31. H. Yan, J.G. Lenard, A study of warm and cold roll-bonding of an aluminium alloy. Mater. Sci. Eng. A. **385**(1–2), 419–428 (2004)
32. R. Jamaati, M.R. Toroghinejad, Investigation of the parameters of the cold roll bonding (CRB) process. Mater. Sci. Eng. A. **527**(9), 2320–2326 (2010)
33. H. Kawamoto, S. Miura, K. Yano, K. Ohkubo, T. Mohri, Analysis of strain transfer through the Mg/Ti interface using crystallographic orientation analysis based on electron back-scattered diffraction patterns. Mater. Trans. **49**(5), 1107–1111 (2008)
34. G.F. Vander Voort, S.R. Lampman, B.R. Sanders, G.J. Anton, C. Polakowski, J. Kinson, K. Muldoon, S.D. Henry, W.W. Scott Jr., ASM handbook. Metallography and microstructures 9. ASM handbook, Materials Park. **9**, 44073–50002 (2004)
35. N. Kashaev et al., Comparative study of mechanical properties using standard and micro-specimens of base materials Inconel 625, Inconel 718 and Ti-6Al-4V. J. Mater. Res. Technol. **2**(1), 43–47 (2013)

36. M.T. Pérez-Prado, D. Valle, O.A. Ruano, Grain refinement of Mg–Al–Zn alloys via accumulative roll bonding. Scripta Mater. **51**(11), 1093–1097 (2004)
37. A.A. Roostaei et al., An investigation into the mechanical behavior and microstructural evolution of the accumulative roll bonded AZ31 Mg alloy upon annealing. Mater. Des. **32**(5), 2963–2968 (2011)
38. S. Sankaranarayanan, S. Jayalakshmi, M. Gupta, Effect of addition of mutually soluble and insoluble metallic elements on the microstructure, tensile and compressive properties of pure magnesium. Mater. Sci. Eng., A. **530**, 149–160 (2011)
39. S.F. Hassan, M. Gupta, Effect of particulate size of Al_2O_3 reinforcement on microstructure and mechanical behavior of solidification processed elemental Mg. J. Alloy. Compd. **419**(1–2), 84–90 (2006)
40. J. Kuśnierz, J. Bogucka, Accumulative roll-bonding (ARB) of Al 99.8%. Arch. Metall. Mater. **50**(1), 219–230 (2005)
41. N. Tsuji, Y. Saito, S.H. Lee, Y. Minamino, ARB (Accumulative Roll-Bonding) and other new techniques to produce bulk ultrafine grained materials. Adv. Eng. Mater. **5**(5), 338–344 (2003)
42. H. Utsunomiya et al., Grain refinement of magnesium alloy sheets by ARB using high-speed rolling mill. J. Phys: Conf. Ser. **165**, 012011 (2009)
43. G.K. Meenashisundaram, M. Gupta, Low volume fraction nano-titanium particulates for improving the mechanical response of pure magnesium. J. Alloy. Compd. **593**, 176–183 (2014)
44. S. Seetharaman, Synthesis and characterization of new titanium containing magnesium materials. Doctoral dissertation, 2014.
45. X.M. Wang et al., Processing, microstructure and mechanical properties of Ti6Al4V particles-reinforced mg matrix composites. Acta Metall. Sin. (English Letters). **29**(10), 940–950 (2016)
46. S. Seetharaman, J. Subramanian, M. Gupta, Improving the Mechanical Properties of Mg–5.6Ti–3Al Composite through Nano-Al_2O_3 Addition with Recrystallisation Heat Treatment. J. Eng. Sci. **9**(1), 1–9 (2013)
47. N. Chawla, Y.-L. Shen, Mechanical behavior of particle reinforced metal matrix composites. Adv Eng Mater. **3**(6), 357–370 (2001)
48. Y.L. Xi et al., Titanium alloy reinforced magnesium matrix composite with improved mechanical properties. Scripta Mater. **54**(1), 19–23 (2006)
49. M. Paramsothy et al., Al(2)O(3) nanoparticle addition to commercial magnesium alloys: multiple beneficial effects. Nanomaterials (Basel). **2**(2), 147–162 (2012)
50. M.J. Shen, M.F. Zhang, W.F. Ying, Processing, microstructure and mechanical properties of bimodal size SiCp reinforced AZ31B magnesium matrix composites. J. Magnes. Alloys. **3**(2), 162–167 (2015)
51. S.F. Hassan, M. Gupta, Development of high performance magnesium nano-composites using nano-Al2O3 as reinforcement. Mater. Sci. Eng. A. **392**(1–2), 163–168 (2005)